

Article

CoNi₂O₄ Coated on Activated Carbon Wheat Husk (ACWH) as a Novel Nano-Electrocatalyst for Methanol and Ethanol Electro-Oxidation

Fatemeh Jamali ¹, Majid Seifi ^{1,*} and Mohammad Bagher Askari ^{2,*}¹ Department of Physics, Faculty of Science, University of Guilan, Rasht P.O. Box 41335-1914, Iran² Department of Semiconductor, Institute of Science and High Technology and Environmental Sciences, Graduate University of Advanced Technology, Kerman P.O. Box 7631818356, Iran

* Correspondence: seifi@guilan.ac.ir (M.S.); mbaskari@phd.guilan.ac.ir (M.B.A.)

Abstract: In this paper, for the first time, a CoNi₂O₄ nanocatalyst coated on the surface of activated carbon wheat husk (ACWH) was synthesized in the form of CoNi₂O₄/ACWH through a hydrothermal process. The electrocatalytic activity of this catalyst was evaluated using methanol oxidation reaction (MOR) and ethanol oxidation reaction (EOR) processes for use in anodes of alcohol fuel cells. Adding ACWH, as a cheap carbon biomass with an excellent active surface area, improves the performance of the catalyst in the oxidation of alcohols. The current density of CoNi₂O₄/ACWH in the MOR process is 160 mA/cm² at an optimal methanol concentration of 2 M; this oxidation current density in the EOR process and at a concentration of 1.5 M ethanol is 150 mA/cm². The stability of CoNi₂O₄/ACWH in MOR and EOR processes, after 1000 consecutive CV cycles, is 98.6% and 94.6%, respectively.

Keywords: CoNi₂O₄; activated carbon wheat husk; methanol oxidation; ethanol oxidation

Citation: Jamali, F.; Seifi, M.; Askari, M.B. CoNi₂O₄ Coated on Activated Carbon Wheat Husk (ACWH) as a Novel Nano-Electrocatalyst for Methanol and Ethanol Electro-Oxidation. *Coatings* **2023**, *13*, 1124. <https://doi.org/10.3390/coatings13061124>

Academic Editor: Gianfranco Carotenuto

Received: 19 February 2023

Revised: 19 March 2023

Accepted: 14 June 2023

Published: 19 June 2023



Copyright: © 2023 by the authors. Licensee MDPI, Basel, Switzerland. This article is an open access article distributed under the terms and conditions of the Creative Commons Attribution (CC BY) license (<https://creativecommons.org/licenses/by/4.0/>).

1. Introduction

Today, energy demand is increasing continuously in the advanced and developing world [1]. Limited sources of fossil fuels not only lead to global energy and fuel shortages, but also endanger human lives due to the enhanced amounts of greenhouse gases and consequences of environmental change [2,3]. A low-cost and environmentally friendly fuel could be used as a suitable alternative to fossil fuels to overcome this problem. There is no doubt that using sustainable and renewable fuel sources, such as sunlight, wind power, geothermal power, etc., is a wise solution for overcoming the energy crisis across the world [4,5].

Reviewing the yearly statistics and data of developed countries on their use of renewable fuel sources indicates that countries allocate enormous budgets for this purpose yearly [6,7]. Although almost all countries have access to renewable and clean energy sources, the production and industrialization of energy transformation to be used in this field need special technical and technological knowledge [8,9]. As an example, a specific photovoltaic cell should be designed and constructed in each location to exploit electric energy from sunlight with the minimum cost and maximum efficiency; the same is true for other cases like wind turbines, devices, and equipment for using sea waves and geothermal energy.

In recent years, with the considerable advancements in nanoscience in energy storage and production, we have witnessed the industrialization of some equipment in this field, such as supercapacitors, various electrochemical batteries, and fuel cells, which are very appealing to customers due to being portable and having small sizes [10,11]. Furthermore, extensive equipment applications in different fields, including pharmaceutical, military, etc., have made developed countries allocate a suitable budget to this field.

Among the mentioned equipment, supercapacitors and electrochemical batteries are used for energy storage [12,13], and fuel cells directly produce energy by transforming

chemical energy into electrical power [14]. One of the advantages of fuel cells is the production of water as a side product [15]. Nowadays, fuel cells have found a special place in energy production. In addition to being clean and efficient, they can be used in any application that needs energy since they can produce 1 W to 10 MW power [16]. Fuel cells are divided into high- and low-temperature cells; alcoholic fuel cells comprise low-temperature cells [17]. Among the different alcohols, methanol and ethanol are significant sources of energy production due to their high energy density, availability, and easy storage and transportation [18–20].

Alcoholic fuel cells consist of three main parts: the anode, cathode, and membrane [21,22]. Fuel electrochemical oxidation occurs on the anode and oxygen reduction occurs on the cathode [23]. One of the parameters that determines the effectiveness of cell efficiency is the structure of the anode electrode, which is responsible for the alcohol oxidation process. Although platinum-based electrocatalysts [24,25], composites, and composite-based hybrids [26–30] have the maximum catalytic activity in alcohol oxidation, their high cost and limited availability are among the challenges of the practical utilization of fuel cells [31]. Other metals, except platinum, with electrocatalytic properties, are ruthenium, palladium, rhenium, and gold [32–34].

Examples of catalyst applications, especially metal oxide-based catalysts, include the use of catalysts based on nickel and cobalt in oxygen evolution reaction (OER) and hydrogen evolution reaction (HER) processes. This broad application of catalysts has attracted much attention recently and has been highly welcomed by researchers [35–37]. The electrode material is a crucial factor in methanol fuel cells due to their slow reaction kinetics. The structure of the electrode material plays an essential role in its electrocatalytic activity. This material should be electrically conductive, with a suitable effective surface area and adequate electrocatalytic activity [38,39].

Metal oxides were studied as electrodes and catalyst materials that can be theoretically applied to electrochemical processes. However, these materials have low electric conductivity and effective surface area. Various methods are reported to improve the performance of metal oxides. Doping or compositing these materials with efficient and precious catalysts like platinum and palladium, or hybridizing metal oxides with surface-active and conductive materials such as MOF, conductive polymers, etc., are among the proposed methods [40–43].

One of the most attractive, cost-effective, and efficient methods of improving the electrocatalytic activity of metal oxides is using carbon in their structures. Various types of carbonaceous material, such as graphene oxide nanotubes and hollow carbon nanospheres (HCNs), facilitate electrochemical processes by increasing their conductivity and improving their catalytic activity [44]. Among the metal oxides, due to the synergistic effect of two metal oxides in one structure in the form of AB_2O_4 , it seems that binary intermediate metal oxides (BTMOs) might be excellent candidates to be used as catalysts in fuel cell structures like $NiCo_2O_4/CuO-C$ [45], $MnNi_2O_4-MWCNTs$ [8], and $MnCo_2O_4/NiCo_2O_4/rGO$ [11].

Among the carbonaceous materials, using the carbon obtained from industrial and agricultural wastes, such as active and conductive carbon, in catalyst structures can be very interesting for scientists. The production processes of these carbons are almost environmentally friendly processes. These carbonaceous materials have attracted much attention due to their availability and low-cost synthesis. Banana fiber [46], rice husk [47], and natural wood [48] are some of these carbons. In this study, wheat husk wastes are used as the source of biomass carbon production, and their combination with $CoNi_2O_4$, as a low-cost and efficient binary metal oxide nanocatalyst, is used in methanol and ethanol oxidation in alcoholic fuel cell anodes. One of the reasons for using wheat husk for carbon production is its abundance and availability, as well as the ease and low cost of preparing biomass carbon from wheat husk waste compared to other materials. According to studies, this type of catalyst, which includes binary metal oxide and biomass carbon, is not used in fuel cell anodes. EIS, LSV, CV, and chronoamperometry analyses of the catalysts have

revealed that $\text{CoNi}_2\text{O}_4/\text{ACWH}$ and CoNi_2O_4 have the ability to oxidize methanol and ethanol. Although both of these catalysts are suitable candidates to be used in alcoholic fuel cell anodes, the presence of ACWH in the CoNi_2O_4 structure improves its electrocatalytic properties due to the active surface and electric conductivity of this carbon.

2. Materials and Methods

All the materials used were Merck Company products with 99% purity. X-ray diffraction (XRD) analysis was performed using an XRD Xpert Pro Panalytical device (Almelo, The Netherlands). FE-SEM ZEISS equipment (GeminiSEM 300, Carl Zeiss, Oberkochen, Germany) was used for FESEM imaging. Raman spectroscopy was performed using Confocal Microscopy (LabRAM ARAMIS, Horiba Jobin Yvon, Longjumeau, France). All the electrochemical analyses were carried out using Potentiostat/Galvanostat Autolab 302 N (Metrohm, Herisau, Switzerland) with a three-electrode system.

2.1. Synthesis of Carbon Biomass

A total of 50 g of pure wheat husk was poured into 450 mL of 1 M nitric acid (HNO_3) and left for one day under stirring; then, it was dried at 60 °C. The product was poured into 500 mL of 1 M NaOH and stirred for 24 h; then, it was dried at 65 °C. The dried product was put in a 400 °C furnace for 3 h. The obtained black material was mixed with 300 mL of 1 M NaOH and stirred for 30 min. The product was dried at 70 °C. The obtained material was mixed with KOH in a 1:4 ratio (WHC/KOH) and put in a CVD at 800 °C. After an acid wash, the powder reached pH 7, and the activated carbon prepared from the wheat husk (ACWH) was ready.

2.2. Synthesis of CoNi_2O_4 and $\text{CoNi}_2\text{O}_4/\text{ACWH}$

The hydrothermal method was used to synthesize CoNi_2O_4 and $\text{CoNi}_2\text{O}_4/\text{ACWH}$. For this purpose, 0.581 g nickel nitrate hexahydrate and 0.291 g cobalt hexahydrate molecules were poured into 15 mL of deionized water and stirred. Then, 3.60 g urea was added to the solution and stirred for 45 min. The resultant homogeneous solutions were placed in a 40 mL autoclave for 12 h at 90 °C. Then, the dilute product was washed with water and ethanol and dried at 80 °C. The obtained powder was annealed at 400 °C.

The $\text{CoNi}_2\text{O}_4/\text{ACWH}$ was prepared using a similar method, with the difference that nickel and cobalt nitrate hexahydrates were added to 10 mL deionized water and mixed with urea. Then, 0.001 g of ACWH that was sonicated in 10 mL water was added to the solution and placed in an autoclave with a similar temperature and conditions to those of the synthesis process; the preparation procedure for the powdered product was then followed. The formation mechanism of the CoNi_2O_4 nanocatalyst was as follows:



2.3. Preparation of Electrode

A setup was prepared to investigate the catalysts' behavior in methanol and ethanol oxidation reactions to be used in alcoholic fuel cell anodes. For this purpose, some slurries containing 0.4 g each of CoNi_2O_4 and $\text{CoNi}_2\text{O}_4/\text{ACWH}$ catalyst in 0.5 mL Naphion 5% and 0.5 mL isopropyl alcohol were separately prepared with ultrasonication for 30 min to disperse the particles completely. An amount of 0.6 μL of this slurry was poured on the surface of the GCE electrode using a micropipette. The electrochemical tests were performed after drying. The electrode system used in this study consisted of a glass carbon electrode (GCE) that was modified by the catalysts to be used as the working electrode. The auxiliary and reference electrodes were a platinum rod with a 0.5 mm diameter and a Ag/AgCl electrode, respectively.

3. Results

3.1. X-ray Diffraction (XRD)

To study the structure and confirm the successful synthesis of nanocatalysts, their crystalline structure was investigated via X-ray diffraction analysis. Figure 1 shows the X-ray diffraction of nanocatalysts and ACWH. As seen in this figure, two intensive peaks of CoNi_2O_4 and $\text{CoNi}_2\text{O}_4/\text{ACWH}$ appeared at about 38 and 44 degrees. Also, one peak was observed at 29 degrees in the ACWH diffraction pattern. The diffraction patterns of CoNi_2O_4 and $\text{CoNi}_2\text{O}_4/\text{ACWH}$ comply with JCPDS No. 00.040.1191. The characteristic peaks of CoNi_2O_4 and $\text{CoNi}_2\text{O}_4/\text{ACWH}$ were occurred at 18.801, 31.005, 38.269, 44.508, 55.187, 58.930, 64.779, and 76.707 degrees, and are related to the Miller planes of (111), (220), (222), (400), (422), (511), (440), and (533), respectively. A comparison of the two diffraction patterns of CoNi_2O_4 and $\text{CoNi}_2\text{O}_4/\text{ACWH}$ indicates that $\text{CoNi}_2\text{O}_4/\text{ACWH}$ peaks have lower intensity at the (220), (222), and (400) Miller planes, which is due to the presence of ACWH in the crystal structure.

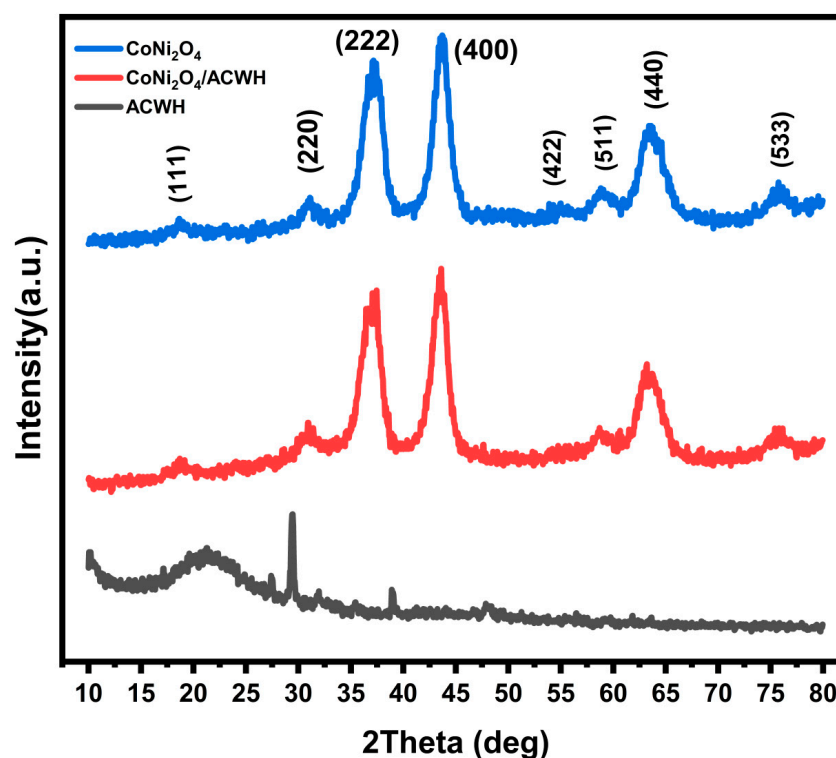


Figure 1. XRD pattern of synthesized CoNi_2O_4 , $\text{CoNi}_2\text{O}_4/\text{ACWH}$, and ACWH.

3.2. FE-SEM

The surface morphology of the prepared nanocatalysts was investigated via Field Emission Scanning Electron Microscopy (FESEM) images. Figure 2 shows the FESEM images of CoNi_2O_4 , $\text{CoNi}_2\text{O}_4/\text{ACWH}$, and ACWH nanoparticles. Figure 2a–c show images from the CoNi_2O_4 nanocatalyst which were taken at 100 nm, 200 nm, and 1 μm , respectively. A surface with contiguous spheres with relatively homogeneous sizes is observed in the picture. Figure 2d–f show images of the $\text{CoNi}_2\text{O}_4/\text{ACWH}$ nanocatalyst; as seen, there is a smooth surface consisting of separate spheres that are attached to nanorods, and the surface particles are at a long distance from each other compared to the nanocatalysts. Figure 2g–i present images taken from ACWH that show a porous surface consisting of nanoparticles and nanosheets.

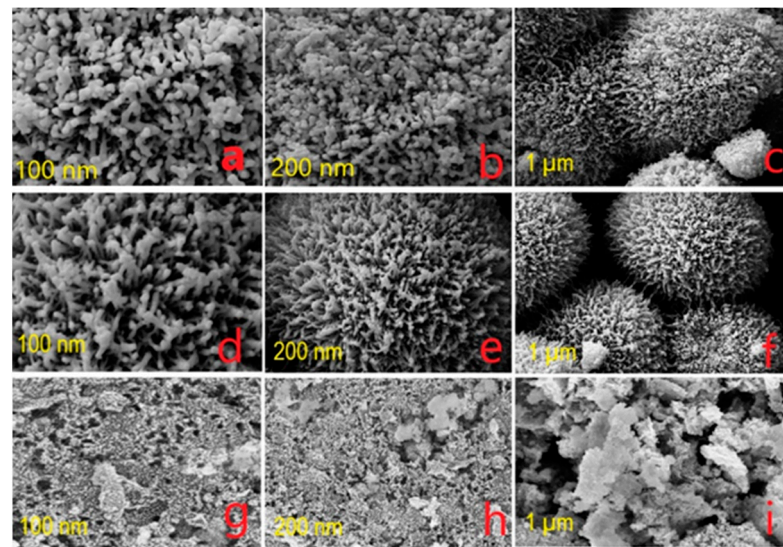


Figure 2. SEM images of CoNi_2O_4 (a–c), $\text{CoNi}_2\text{O}_4/\text{ACWH}$ (d–f), and ACWH (g–i) at different magnifications.

3.3. EDX-Mapping

EDX-mapping elemental analysis was used to identify the composition of CoNi_2O_4 and $\text{CoNi}_2\text{O}_4/\text{ACWH}$ nanocatalysts. As seen in Figures 3 and 4, Co, O, Ni, and C elements are present in the synthesized nanostructures. According to mapping images of CoNi_2O_4 nanocatalyst in Figure 3a, the presence of Co, Ni, and O elements is confirmed. Besides, the mapping images of $\text{CoNi}_2\text{O}_4/\text{ACWH}$ in Figure 3b indicate the presence and uniform distribution of Co, Ni, O, and C elements.

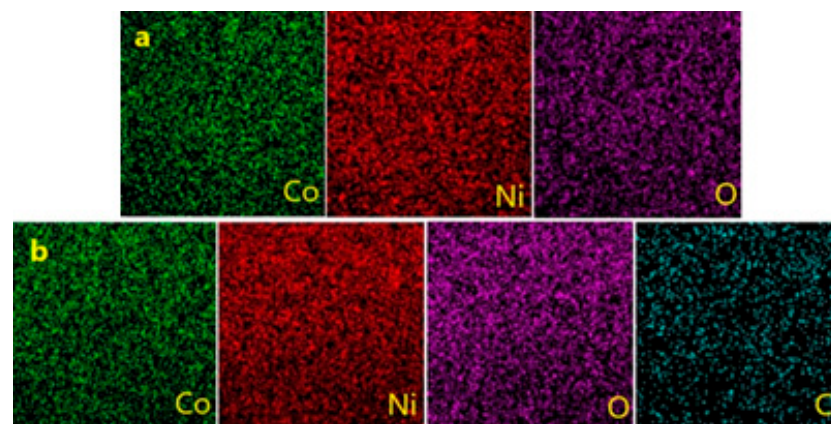


Figure 3. Mapping analysis of CoNi_2O_4 (a) and $\text{CoNi}_2\text{O}_4/\text{ACWH}$ (b).

3.4. Raman Spectroscopy

Raman spectroscopy is used for the structural study of the nanocatalysts to confirm the presence of carbon in their structures. Figure 5 presents the Raman spectra of the nanocatalysts. Two peaks with high resolution are observed in the Raman spectra of the nanocatalyst containing ACWH that are related to the D and G bands of carbon. Bond D in the 1300 to 1400 (cm^{-1}) range belongs to carbonaceous atoms that experienced irregularity. Bond G at about 1600 (cm^{-1}) is related to the E_{2g} state of the graphite structure. These two peaks confirm the carbonaceous and graphene structure of ACWH, which are evident in the Raman spectra of the $\text{CoNi}_2\text{O}_4/\text{ACWH}$ nanocatalyst and indicate the presence of ACWH in this structure.

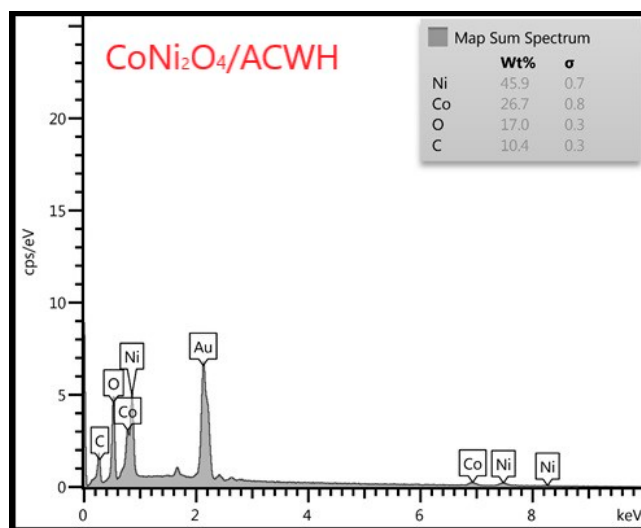


Figure 4. EDX analysis of $\text{CoNi}_2\text{O}_4/\text{ACWH}$.

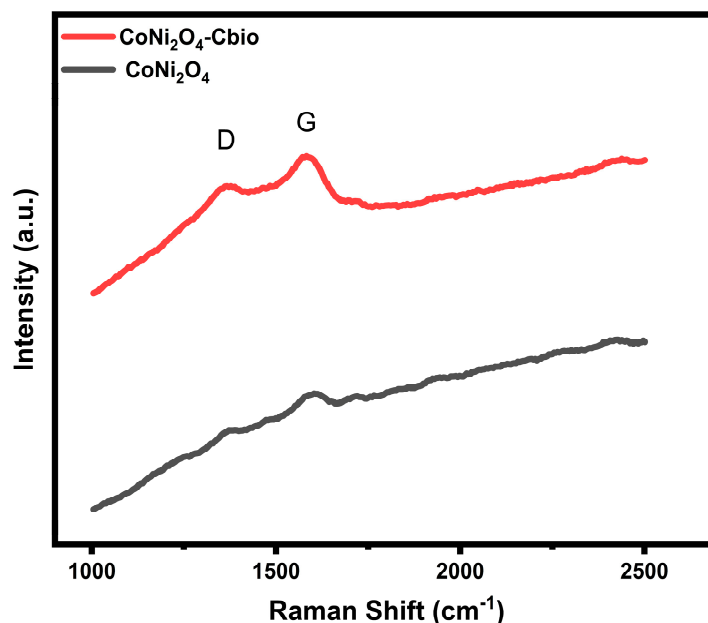


Figure 5. Raman spectra of $\text{CoNi}_2\text{O}_4/\text{ACWH}$ and CoNi_2O_4 .

3.5. BET Method

The BET method is used to check the specific surface area and porosity of samples based on nitrogen adsorption and desorption isotherms at a nitrogen boiling temperature of 77 degrees Kelvin. Figure 6 shows the adsorption–desorption isotherms of the CoNi_2O_4 and $\text{CoNi}_2\text{O}_4/\text{ACWH}$ samples. According to the IUPAC isotherms, the CoNi_2O_4 and $\text{CoNi}_2\text{O}_4/\text{ACWH}$ isotherms are of type IV, which shows that the samples have a mesoporous structure and the relationship between the surface of the sample and the adsorbent is relatively strong. Investigating the CoNi_2O_4 and $\text{CoNi}_2\text{O}_4/\text{ACWH}$ isotherms indicated that adding ACWH to CoNi_2O_4 increases the specific surface area. Based on the results obtained from the analysis, the specific surface area of CoNi_2O_4 and $\text{CoNi}_2\text{O}_4/\text{ACWH}$ nanocatalysts is 69.686 and 75.089 m^2/g , respectively. These results confirm the claim that by increasing the effective level of the catalyst, the performance of the catalyst improves, and these results can be attributed to the addition of ACWH to the CoNi_2O_4 catalyst.

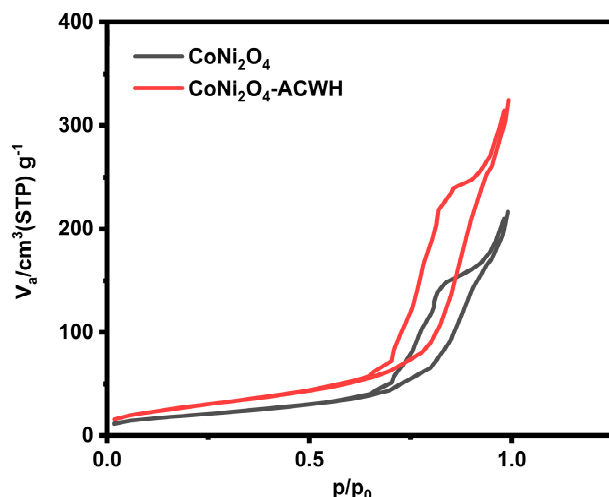


Figure 6. BET of CoNi₂O₄/ACWH and CoNi₂O₄.

3.6. Electrochemical Studies

3.6.1. Investigation of CoNi₂O₄ and CoNi₂O₄/ACWH Nanocatalysts’ Abilities in Methanol Oxidation Process

As far as we know, metal oxides exhibit maximum efficiency in alcohol oxidation processes in alkaline environments. A 0.5 M KOH solution was prepared, and cyclic voltammetry (CV) analysis was carried out on the modified electrodes with CoNi₂O₄ and CoNi₂O₄/ACWH, at a scan rate of 20 mV/s. The results are presented in Figure 7a. As seen, CoNi₂O₄/ACWH has a higher capacitive current density due to its higher electrical conductivity and more electrochemically active surface compared to CoNi₂O₄. The reason for this superiority is the presence of biomass carbon from the wheat husk in the CoNi₂O₄/ACWH structure. The results of the Electrochemical Impedance Spectroscopy (EIS) analysis of CoNi₂O₄ and CoNi₂O₄/ACWH catalysts, in the frequency range of 1 MHz to 10 KHz, are presented in Figure 7b. The resistance against charge transfer for CoNi₂O₄ and CoNi₂O₄/ACWH is 30.5 and 18.2 Ω, respectively, which shows the positive effect of carbon biomass present in the catalysts’ structure.

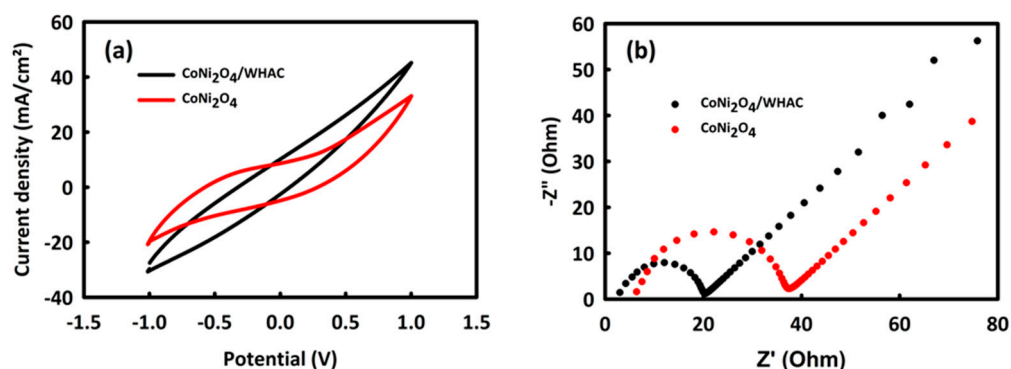


Figure 7. CV (a) and EIS (b) analysis of CoNi₂O₄ and CoNi₂O₄/WHAC in 0.5 M KOH.

To investigate the behavior of CoNi₂O₄ and CoNi₂O₄/ACWH in the methanol oxidation process, some solutions were prepared containing 0.5 M KOH and various methanol concentrations (0.5–3 M). As can be seen in the CV analysis of the two nanocatalysts, in the potential range of 0–0.8 V and at a scan rate of 20 mV/s, enhanced methanol concentration causes an increase in the current density of the electrode that was modified with CoNi₂O₄. This enhancement in the current density continues up to a 1.5 M concentration, a further increase in the concentration causes a reduction in current density, and the oxidation peak has a descending trend. The same trend is observed in CoNi₂O₄/ACWH; the current den-

sity of the methanol oxidation peak increases up to a methanol concentration of 2 M, but lower current density is observed at higher concentrations. It seems that the nanocatalyst surface becomes saturated at a concentration higher than the optimum concentration, and electrolyte/methanol cannot penetrate easily to the catalyst core; this causes a reduction in current density. The behavior of CoNi_2O_4 and $\text{CoNi}_2\text{O}_4/\text{ACWH}$ nanocatalysts at different methanol concentrations is presented in Figure 8a,b.

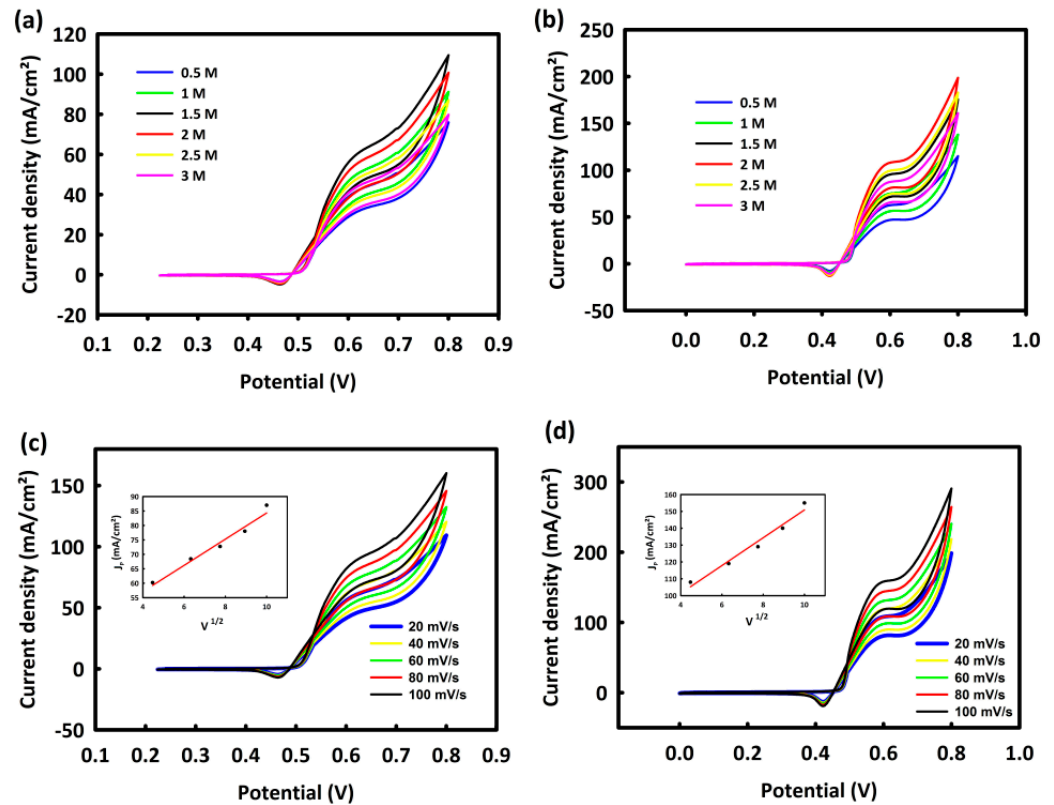
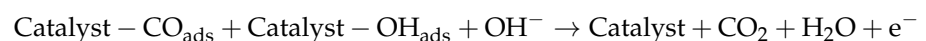
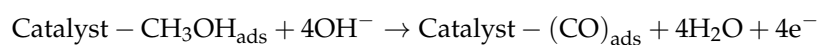
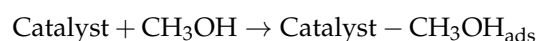


Figure 8. CV from CoNi_2O_4 (a) and $\text{CoNi}_2\text{O}_4/\text{ACWH}$ (b) in 0.5 M KOH/different concentrations of methanol. CV from CoNi_2O_4 (c) and $\text{CoNi}_2\text{O}_4/\text{ACWH}$ (d) in 0.5 M KOH/optimal concentration of methanol/at different scan rates. The plots of the square root of scan rate in terms of peak current density (J_p) for CoNi_2O_4 and $\text{CoNi}_2\text{O}_4/\text{ACWH}$ are shown in insets of (c,d).

The CV analysis was carried out at different scan rates of 20 to 100 mV/s to study the methanol oxidation mechanism of CoNi_2O_4 and $\text{CoNi}_2\text{O}_4/\text{ACWH}$. An enhanced current density of the oxidative peak was observed for CoNi_2O_4 and $\text{CoNi}_2\text{O}_4/\text{ACWH}$ after increasing the scan rate. This ascending trend is presented in Figure 8c,d, respectively. The square of the scan rate as a function of peak current density (J_p) is shown in the insets of these figures. The linear relationship between these two parameters, with $R^2 = 0.996$ and $R^2 = 0.991$, indicates that diffusion is the controlling mechanism of methanol oxidation by CoNi_2O_4 and $\text{CoNi}_2\text{O}_4/\text{ACWH}$. The proposed six-electron mechanism for these nanocatalysts is in the following form [49]:



The stability of CoNi_2O_4 and $\text{CoNi}_2\text{O}_4/\text{ACWH}$ nanocatalysts in methanol oxidation can be assessed via CV. The CoNi_2O_4 nanocatalyst shows 95.8% stability after 1000 consecutive CV cycles at 0.5 KOH/1.5 methanol solution at a scanning rate of 100 mV/s (Figure 9a), while $\text{CoNi}_2\text{O}_4/\text{ACWH}$ shows 98.6% stability after the same number of cycles and the same scan rate, but in 0.5 KOH/2 methanol solution (Figure 9b).

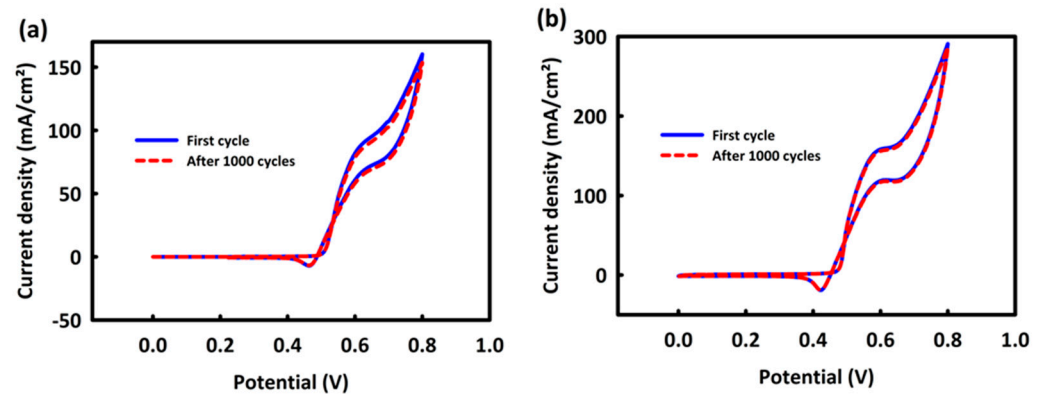


Figure 9. Cyclic stability for CoNi_2O_4 (a) and $\text{CoNi}_2\text{O}_4/\text{ACWH}$ (b) in MOR process after 1000 consecutive CV cycles.

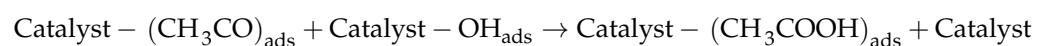
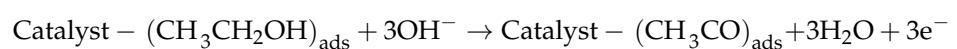
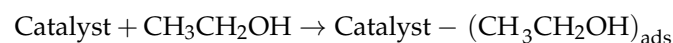
3.6.2. Investigation of CoNi_2O_4 and $\text{CoNi}_2\text{O}_4/\text{ACWH}$ Nanocatalyst Capabilities in Ethanol Oxidation Process for Use in Ethanol Fuel Cells

To investigate the capability of CoNi_2O_4 and $\text{CoNi}_2\text{O}_4/\text{ACWH}$ nanocatalysts in the oxidation of ethanol in an alkaline environment, various amounts of ethanol were added to KOH 0.5 M, and CV analysis was performed at a 20 mV/s scan rate and in the potential range of 0–0.8 V. Figure 10a shows CoNi_2O_4 nanocatalyst behavior and Figure 10b shows $\text{CoNi}_2\text{O}_4/\text{ACWH}$ nanocatalyst behavior at different ethanol concentrations. The surfaces of CoNi_2O_4 and $\text{CoNi}_2\text{O}_4/\text{ACWH}$ nanocatalysts become saturated at 1 and 1.5 M ethanol concentrations, and the oxidative peak of current density undergoes a descending trend at higher ethanol concentrations. Here, it also seems that the catalyst surface became saturated at concentrations higher than the critical concentration, and ethanol could not penetrate the depth of the catalyst anymore.

The methanol oxidation mechanism of CoNi_2O_4 and $\text{CoNi}_2\text{O}_4/\text{ACWH}$ nanocatalysts was determined via a CV test at the optimum ethanol concentration and a scan rate of 10–100 mV/s. Figure 10c,d show the behavior of CoNi_2O_4 and $\text{CoNi}_2\text{O}_4/\text{ACWH}$ nanocatalysts at different scan rates. An increase in anodic current density is observed with increasing scan rate.

The squared scan rate as a function of the peak current density (J_p) is presented in the insets of these figures. The linear relationship of these two parameters with $R^2 = 0.994$ and $R^2 = 0.996$ for CoNi_2O_4 and $\text{CoNi}_2\text{O}_4/\text{ACWH}$, respectively, implies that diffusion is the controlling mechanism in the EOR process.

The proposed mechanism for ethanol oxidation can be expressed in the following form:



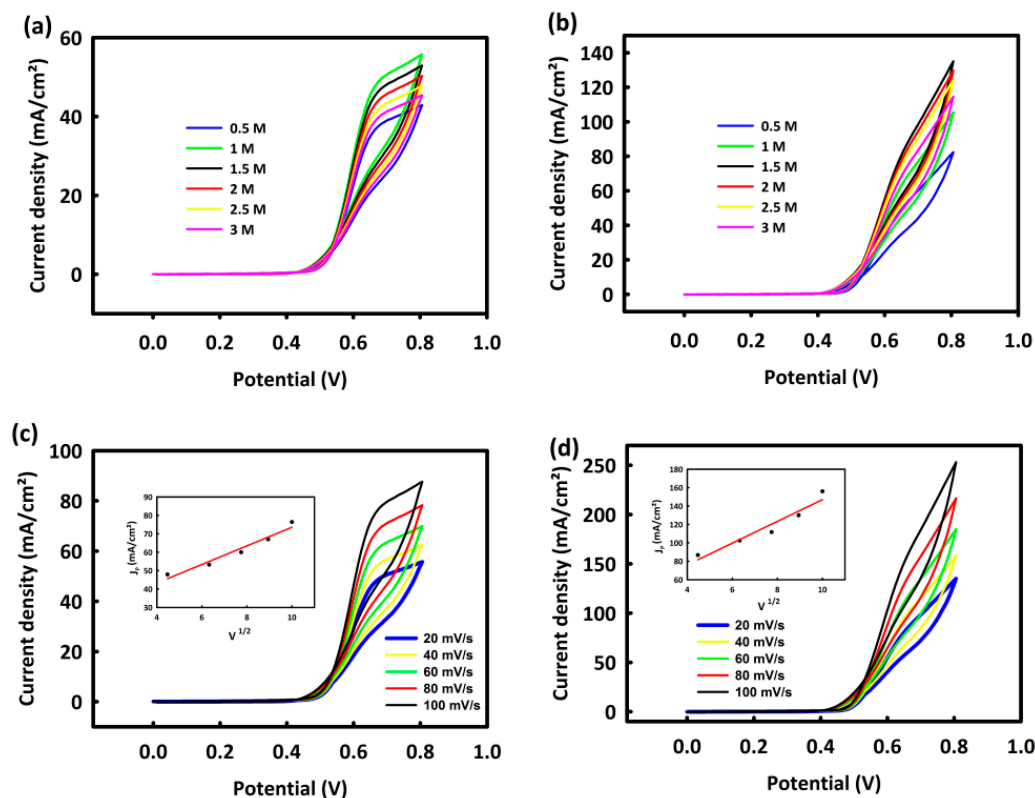


Figure 10. CV from CoNi₂O₄ (a) and CoNi₂O₄/ACWH (b) in 0.5 M KOH/different concentrations of ethanol. CV from CoNi₂O₄ (c) and CoNi₂O₄/ACWH (d) in 0.5 M KOH/optimal concentration of ethanol/at different scan rates. The plots of the square root of the scan rate in terms of maximum current density for CoNi₂O₄ and CoNi₂O₄/ACWH are shown in insets of (c,d).

The stability of CoNi₂O₄ and CoNi₂O₄/ACWH nanocatalysts in the EOR process was evaluated through 1000 consecutive CV analyses at the optimum ethanol concentration and a scan rate of 60 mV/s. Figure 11a,b present the cyclic stability of CoNi₂O₄ and CoNi₂O₄/ACWH. After these cycles, a stability of 91.5% for CoNi₂O₄ and 94.6% for CoNi₂O₄/ACWH is obtained.

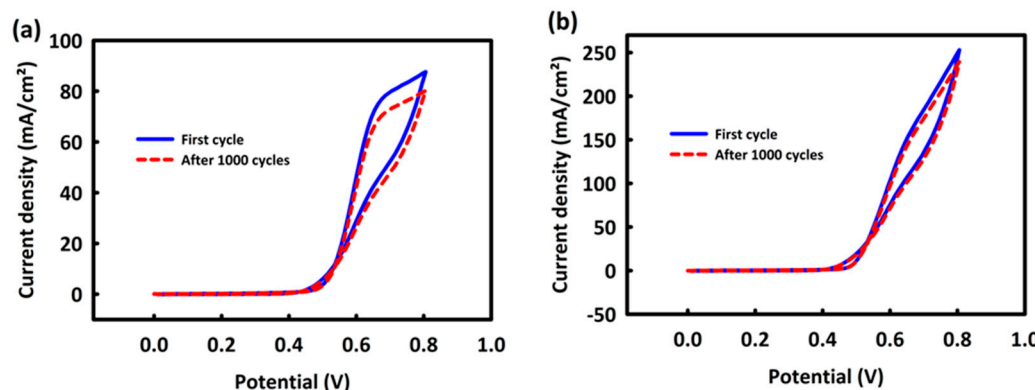


Figure 11. Cyclic stability of CoNi₂O₄ (a) and CoNi₂O₄/ACWH (b) in MOR process after 1000 consecutive CV cycles.

In Table 1, we compare the performance and efficiency of CoNi₂O₄/ACWH nanocatalyst in the MOR and EOR processes with other recent research.

Table 1. Comparison of MOR and EOR performance of CoNi₂O₄/ACWH nanocatalyst with other recent research.

Electrocatalyst	Electrolyte Composition	Peak Potential (V)	Current Density (mA cm ⁻²)	Scan Rate (mV/s)	Reference
CoNi ₂ O ₄ /ACWH	2 M methanol/0.5 M KOH	0.58	160	60	This work
CoNi ₂ O ₄ /ACWH	1.5 M ethanol/0.5 M KOH	0.63	150	60	This work
ZrO ₂ /NiO/rGO	0.7 M methanol/0.5 M KOH	0.52	26.6	20	[10]
ZrO ₂ /NiO/rGO	0.5 M ethanol/0.5 M KOH	0.52	17.3	20	[10]
Mn ₃ O ₄ -CeO ₂ -rGO	0.8 M methanol/1 M KOH	0.51	17.7	90	[49]
Ni ₃ S ₄ -NiS-rGO	0.7 M methanol/1 M KOH	0.54	55	80	[50]
Ni ₃ S ₄ -NiS-rGO	0.5 M ethanol/1 M KOH	0.59	11	60	[50]
NiCo ₂ O ₄	0.5 M methanol/1 M KOH	0.7	129	10	[51]
NiCo ₂ O ₄ /carbon xerogel	0.5 M methanol/0.5 M KOH	0.29	98	50	[52]
3D Ni/NiO/RG	1 M methanol/1 M KOH	About 0.6	79.21	50	[53]
NiO 2.5CeO ₂ -NiO	1 M methanol/1 M KOH	About 0.55	159.62	50	[54]
Cu-Ni/CuO-NiO/GNs	0.5 M methanol/1 M KOH	0.7	150	50	[55]
NiO NS@NW/NF	0.5 M methanol/1 M KOH	1.62	89	10	[56]
PEDOT:PSS/MnO ₂ /rGO	0.5 M methanol/1 M NaOH	0.32	56.38	50	[57]

4. Conclusions

In this research study, CoNi₂O₄ and CoNi₂O₄/ACWH nanocatalysts were synthesized and their capabilities in the oxidation of methanol and ethanol, to be used in alcohol fuel cell anodes, were investigated. The CoNi₂O₄/ACWH nanocatalyst was more efficient than the CoNi₂O₄ nanocatalyst, and its higher efficiency was due to the presence of synthesized biomass from the wheat husk in the CoNi₂O₄/ACWH structure. The synthesized carbon with a large active surface and acceptable electric conductivity provides a higher catalytic surface for methanol and ethanol and facilitates the oxidation of these two alcohols by the catalyst. In methanol oxidation at a scan rate of 100 mV/s, CoNi₂O₄/ACWH had an oxidative current density of 160 mA/cm² at the excessive potential of 0.58 V, and its stability was 98.6% after 1000 consecutive CV cycles. CoNi₂O₄/ACWH was also a cost-effective and stable catalyst for ethanol oxidation; its stability was 94.6% after 1000 consecutive CV cycles. The oxidative current density for this nanocatalyst was 150 mA/cm² at ethanol oxidation with a peak voltage of 0.63 V. This is the first time that the proposed nanocatalysts have been assessed in MOR and EOR processes, and the results are promising regarding their application in alcoholic fuel cells.

Author Contributions: Conceptualization, F.J., M.S. and M.B.A.; data curation F.J.; formal analysis, F.J. and M.B.A.; funding acquisition M.S. and M.B.A.; investigation, F.J. and M.B.A.; methodology, F.J., M.B.A. and M.S.; resources, M.B.A.; software, F.J. and M.S.; supervision, M.S. and M.B.A.; validation, M.B.A.; visualization, F.J.; writing—original draft, F.J. and M.B.A.; writing—review and editing, M.S. All authors have read and agreed to the published version of the manuscript.

Funding: This research received no external funding.

Institutional Review Board Statement: Not applicable.

Informed Consent Statement: Not applicable.

Data Availability Statement: The data are available upon request from the authors.

Conflicts of Interest: The authors declare no conflict of interest.

References

- Bahrapour, H.; Marnani, A.K.B.; Askari, M.B.; Bahrapour, M.R. Evaluation of renewable energies production potential in the Middle East: Confronting the world's energy crisis. *Front. Energy* **2017**, *14*, 42–56. [\[CrossRef\]](#)
- Singh, S. *Energy Crisis and Climate Change: Global Concerns and Their Solutions, Energy: Crises, Challenges and Solutions*; John Wiley & Sons: Hoboken, NJ, USA, 2021; pp. 1–17.
- Shen, M.; Huang, W.; Chen, M.; Song, B.; Zeng, G.; Zhang, Y. (Micro)plastic crisis: Un-ignorable contribution to global greenhouse gas emissions and climate change. *J. Clean. Prod.* **2020**, *254*, 120138. [\[CrossRef\]](#)

4. Shojaeifar, M.; Askari, M.B.; Hashemi, S.R.S.; Di Bartolomeo, A. MnO₂-NiO-MWCNTs nanocomposite as a catalyst for methanol and ethanol electrooxidation. *J. Phys. D Appl. Phys.* **2022**, *55*, 355502. [[CrossRef](#)]
5. Bhuiyan, M.R.A.; Mamur, H.; Begum, J. A brief review on renewable and sustainable energy resources in Bangladesh. *Clean. Eng. Technol.* **2021**, *4*, 100208. [[CrossRef](#)]
6. Shang, Y.; Razzaq, A.; Chupradit, S.; An, N.B.; Abdul-Samad, Z. The role of renewable energy consumption and health expenditures in improving load capacity factor in ASEAN countries: Exploring new paradigm using advance panel models. *Renew. Energy* **2022**, *191*, 715–722. [[CrossRef](#)]
7. Aslanturk, O.; Kiprizli, G. The role of renewable energy in ensuring energy security of supply and reducing energy-related import. *Int. J. Energy Econ. Policy* **2020**, *10*, 354–359. [[CrossRef](#)]
8. Hosseini, S.; Askari, M.B.; Beitollahi, H. MnNi₂O₄-MWCNTs as a nano-electrocatalyst for methanol oxidation reaction. *Int. J. Hydrogen Energy* **2022**, *48*, 21240–21248. [[CrossRef](#)]
9. Azarpour, A.; Mohammadzadeh, O.; Rezaei, N.; Zendehboudi, S. Current status and future prospects of renewable and sustainable energy in North America: Progress and challenges. *Energy Convers. Manag.* **2022**, *269*, 115945. [[CrossRef](#)]
10. Askari, M.B.; Beitollahi, H.; Di Bartolomeo, A. Methanol and Ethanol Electrooxidation on ZrO₂/NiO/rGO. *Nanomaterials* **2023**, *13*, 679. [[CrossRef](#)]
11. Askari, M.B.; Azizi, S.; Moghadam, M.T.T.; Seifi, M.; Rozati, S.M.; Di Bartolomeo, A. MnCo₂O₄/NiCo₂O₄/rGO as a Catalyst Based on Binary Transition Metal Oxide for the Methanol Oxidation Reaction. *Nanomaterials* **2022**, *12*, 4072. [[CrossRef](#)] [[PubMed](#)]
12. Olabi, A.G.; Abbas, Q.; Al Makky, A.; Abdelkareem, M.A. Supercapacitors as next generation energy storage devices: Properties and applications. *Energy* **2022**, *248*, 123617. [[CrossRef](#)]
13. Iqbal, M.Z.; Aziz, U. Supercapattery: Merging of battery-supercapacitor electrodes for hybrid energy storage devices. *J. Energy Storage* **2022**, *46*, 103823. [[CrossRef](#)]
14. Kaur, A.; Kaur, G.; Singh, P.P.; Kaushal, S. Supported bimetallic nanoparticles as anode catalysts for direct methanol fuel cells: A review. *Int. J. Hydrogen Energy* **2021**, *46*, 15820–15849. [[CrossRef](#)]
15. Okonkwo, P.C.; Otor, C. A review of gas diffusion layer properties and water management in proton exchange membrane fuel cell system. *Int. J. Energy Res.* **2020**, *45*, 3780–3800. [[CrossRef](#)]
16. Lasseeter, R. Dynamic models for micro-turbines and fuel cells. In Proceedings of the 2001 Power Engineering Society Summer Meeting. Conference Proceedings (Cat. No. 01CH37262), IEEE, Vancouver, BC, Canada, 15–19 July 2001.
17. Yang, B.C.; Koo, J.; Shin, J.W.; Go, D.; Shim, J.H.; An, J. Direct Alcohol-Fueled Low-Temperature Solid Oxide Fuel Cells: A Review. *Energy Technol.* **2018**, *7*, 5–19. [[CrossRef](#)]
18. Salarizadeh, P.; Moghadam, M.T.T.; Askari, M.B. Comparison of methanol oxidation reaction process for NiCo₂O₄/X (X = rGO, MWCNTs, HCNs) nanocatalyst. *Diam. Relat. Mater.* **2023**, *131*, 109534. [[CrossRef](#)]
19. Salarizadeh, P.; Askari, M.B.; Di Bartolomeo, A. MoS₂/Ni₃S₂/Reduced graphene oxide nanostructure as an electrocatalyst for alcohol fuel cells. *ACS Appl. Nano Mater.* **2022**, *5*, 3361–3373. [[CrossRef](#)]
20. Jinxi, W.; Aimin, W.; Ghasemi, A.K.; Lashkenari, M.S.; Pashai, E.; Karaman, C.; Niculina, D.E.; Karimi-Maleh, H. Tailoring of ZnFe₂O₄-ZrO₂-based nanoarchitectures catalyst for supercapacitor electrode material and methanol oxidation reaction. *Fuel* **2023**, *334*, 26685. [[CrossRef](#)]
21. Kim, S.; Ahn, C.; Karuppanan, M.; Sung, Y.; Kwon, O.J.; Cho, Y. Structural modification of electrode for anion exchange membrane fuel cell by controlling ionomer dispersion. *Int. J. Energy Res.* **2021**, *46*, 6471–6479. [[CrossRef](#)]
22. Gong, C.; Zhao, S.; Tsen, W.-C.; Hu, F.; Zhong, F.; Zhang, B.; Liu, H.; Zheng, G.; Qin, C.; Wen, S. Hierarchical layered double hydroxide coated carbon nanotube modified quaternized chitosan/polyvinyl alcohol for alkaline direct methanol fuel cells. *J. Power Sources* **2019**, *441*, 227176. [[CrossRef](#)]
23. Askari, M.B.; Rozati, S.M. Construction of Co₃O₄-Ni₃S₄-rGO ternary hybrid as an efficient nanoelectrocatalyst for methanol and ethanol oxidation in alkaline media. *J. Alloys Compd.* **2021**, *900*, 163408. [[CrossRef](#)]
24. Zhao, G.; Fang, C.; Hu, J.; Zhang, D. Platinum-Based Electrocatalysts for Direct Alcohol Fuel Cells: Enhanced Performances toward Alcohol Oxidation Reactions. *Chempluschem* **2021**, *86*, 574–586. [[CrossRef](#)] [[PubMed](#)]
25. Tian, H.; Yu, Y.; Wang, Q.; Li, J.; Rao, P.; Li, R.; Du, Y.; Jia, C.; Luo, J.; Deng, P.; et al. Recent advances in two-dimensional Pt based electrocatalysts for methanol oxidation reaction. *Int. J. Hydrogen Energy* **2021**, *46*, 31202–31215. [[CrossRef](#)]
26. Yang, C.; Jiang, Q.; Huang, H.; He, H.; Yang, L.; Li, W. Polyelectrolyte-Induced Stereoassembly of Grain Boundary-Enriched Platinum Nanoworms on Ti₃C₂T_x MXene Nanosheets for Efficient Methanol Oxidation. *ACS Appl. Mater. Interfaces* **2020**, *12*, 23822–23830. [[CrossRef](#)]
27. Wei, S.; Zhan, W.; Ma, L.; Gan, M. NiMoO₄ nanorods derives carbon layers wrapped NiCo alloy decorated with Mo₂C platinum-based catalyst for efficient methanol electrooxidation. *J. Alloys Compd.* **2022**, *927*, 166963. [[CrossRef](#)]
28. Wang, H.; Yang, Y.; Ren, Y.; Chen, D.; Wei, J.; Wang, L.; Xie, A.; Luo, S. Electrochemical synthesis of Pt nanoparticles on ZrO₂/MWCNTs hybrid with high electrocatalytic performance for methanol oxidation. *J. Electroanal. Chem.* **2021**, *898*, 115641. [[CrossRef](#)]
29. Vulcu, A.; Radu, T.; Porav, A.; Berghian-Grosan, C. Low-platinum catalyst based on sulfur doped graphene for methanol oxidation in alkaline media. *Mater. Today Energy* **2020**, *19*, 100588. [[CrossRef](#)]

30. Kianfar, S.; Golikand, A.N.; ZareNezhad, B. Bimetallic-metal oxide nanoparticles of Pt-M (M: W, Mo, and V) supported on reduced graphene oxide (rGO): Radiolytic synthesis and methanol oxidation electrocatalysis. *J. Nanostructure Chem.* **2020**, *11*, 287–299. [[CrossRef](#)]
31. Askari, M.B.; Salarizadeh, P.; Beitollahi, H.; Tajik, S.; Eshghi, A.; Azizi, S. Electro-oxidation of hydrazine on NiFe₂O₄-rGO as a high-performance nano-electrocatalyst in alkaline media. *Mater. Chem. Phys.* **2021**, *275*, 125313. [[CrossRef](#)]
32. Hernández, J.; Solla-Gullón, J.; Herrero, E.; Aldaz, A.; Feliu, J.M. Methanol oxidation on gold nanoparticles in alkaline media: Unusual electrocatalytic activity. *Electrochim. Acta* **2006**, *52*, 1662–1669. [[CrossRef](#)]
33. Chrzanowski, W.; Wieckowski, A. Surface structure effects in platinum/ruthenium methanol oxidation electrocatalysis. *Langmuir* **1998**, *14*, 1967–1970. [[CrossRef](#)]
34. Ali, A.; Shen, P.K. Recent advances in graphene-based platinum and palladium electrocatalysts for the methanol oxidation reaction. *J. Mater. Chem. A* **2019**, *7*, 22189–22217. [[CrossRef](#)]
35. Sun, H.; Xu, X.; Kim, H.; Jung, W.; Zhou, W.; Shao, Z. Electrochemical water splitting: Bridging the gaps between fundamental research and industrial applications. *Energy Environ. Mater.* **2023**, e12441. [[CrossRef](#)]
36. Song, S.; Mu, L.; Jiang, Y.; Sun, J.; Zhang, Y.; Shi, G.; Sun, H. Turning Electrocatalytic Activity Sites for the Oxygen Evolution Reaction on Brownmillerite to Oxyhydroxide. *ACS Appl. Mater. Interfaces* **2022**, *14*, 47560–47567. [[CrossRef](#)]
37. Sun, H.; Li, L.; Chen, Y.; Kim, H.; Xu, X.; Guan, D.; Hu, Z.; Zhang, L.; Shao, Z.; Jung, W. Boosting Ethanol Oxidation by NiOOH-CuO Nano-Heterostructure for Energy-Saving Hydrogen Production and Biomass Upgrading. *Appl. Catalysis B Environ.* **2023**, *325*, 122388. [[CrossRef](#)]
38. Zhang, G.; Huang, C.; Qin, R.; Shao, Z.; An, D.; Zhang, W.; Wang, Y. Uniform Pd–Pt alloy nanoparticles supported on graphite nanoplatelets with high electrocatalytic activity towards methanol oxidation. *J. Mater. Chem. A* **2015**, *3*, 5204–5211. [[CrossRef](#)]
39. Hu, Y.; Mei, T.; Li, J.; Wang, J.; Wang, X. Porous SnO₂ hexagonal prism-attached Pd/rGO with enhanced electrocatalytic activity for methanol oxidation. *RSC Adv.* **2017**, *7*, 29909–29915. [[CrossRef](#)]
40. Ye, J.; Cheng, B.; Yu, J.; Ho, W.; Wageh, S.; Al-Ghamdi, A.A. Hierarchical Co₃O₄-NiO hollow dodecahedron-supported Pt for room-temperature catalytic formaldehyde decomposition. *Chem. Eng. J.* **2021**, *430*, 132715. [[CrossRef](#)]
41. Nie, Y.; Wang, Y.; Zheng, X.; Yang, T.; Wen, Q.; Fang, Y.; Cheng, X.; Li, R.; Li, L. Minutely surficial functionalization of Ce-O-Pt linkages on Pt/C for enhanced electrocatalytic methanol oxidation. *Appl. Surf. Sci.* **2022**, *602*, 154194. [[CrossRef](#)]
42. Khalafallah, D.; Alothman, O.Y.; Fouad, H.; Khalil, K.A. Hierarchical Co₃O₄ decorated PPy nanocasting core-shell nanospheres as a high performance electrocatalysts for methanol oxidation. *Int. J. Hydrogen Energy* **2018**, *43*, 2742–2753. [[CrossRef](#)]
43. Askari, M.B.; Salarizadeh, P.; Di Bartolomeo, A.; Zadeh, M.H.R.; Beitollahi, H.; Tajik, S. Hierarchical nanostructures of MgCo₂O₄ on reduced graphene oxide as a high-performance catalyst for methanol electro-oxidation. *Ceram. Int.* **2021**, *47*, 16079–16085. [[CrossRef](#)]
44. Zaiman, N.F.H.N.; Shaari, N. Review on flower-like structure nickel based catalyst in fuel cell application. *J. Ind. Eng. Chem.* **2023**, *119*, 1–76. [[CrossRef](#)]
45. Sheikhi, S.; Jalali, F. Hierarchical NiCo₂O₄/CuO-C nanocomposite derived from copper-based metal organic framework and Ni/Co hydroxides: Excellent electrocatalytic activity towards methanol oxidation. *J. Alloys Compd.* **2022**, *907*, 164510. [[CrossRef](#)]
46. Subramanian, V.; Luo, C.; Stephan, A.M.; Nahm, K.S.; Thomas, S.; Wei, B. Supercapacitors from Activated Carbon Derived from Banana Fibers. *J. Phys. Chem. C* **2007**, *111*, 7527–7531. [[CrossRef](#)]
47. Soltani, N.; Bahrami, A.; Pech-Canul, M.; González, L. Review on the physicochemical treatments of rice husk for production of advanced materials. *Chem. Eng. J.* **2015**, *264*, 899–935. [[CrossRef](#)]
48. Shen, Z.; Feng, J. Preparation of thermally conductive polymer composites with good electromagnetic interference shielding efficiency based on natural wood-derived carbon scaffolds. *ACS Sustain. Chem. Eng.* **2019**, *7*, 6259–6266. [[CrossRef](#)]
49. Askari, N.; Askari, M.B.; Di Bartolomeo, A. Electrochemical Alcohol Oxidation and Biological Properties of Mn₃O₄-Co₃O₄-rGO. *J. Electrochem. Soc.* **2022**, *169*, 106511. [[CrossRef](#)]
50. Azizi, S.; Askari, M.B.; Moghadam, M.T.T.; Seifi, M.; Di Bartolomeo, A. Ni₃S₄/NiS/rGO as a promising electrocatalyst for methanol and ethanol electro-oxidation. *Nano Futur.* **2023**, *7*, 015002. [[CrossRef](#)]
51. Das, A.K.; Jena, S.; Sahoo, S.; Kuchi, R.; Kim, D.; Aljohani, T.; Nayak, G.C.; Jeong, J.-R. Facile synthesis of NiCo₂O₄ nanorods for electrocatalytic oxidation of methanol. *J. Saudi Chem. Soc.* **2020**, *24*, 434–444. [[CrossRef](#)]
52. El-Deeb, M.M.; El Roubi, W.M.; Abdelwahab, A.; Farghali, A.A. Effect of pore geometry on the electrocatalytic performance of nickel cobaltite/ carbon xerogel nanocomposite for methanol oxidation. *Electrochim. Acta* **2018**, *259*, 77–85. [[CrossRef](#)]
53. Zhang, K.; Han, Y.; Qiu, J.; Ding, X.; Deng, Y.; Wu, Y.; Zhang, G.; Yan, L. Interface engineering of Ni/NiO heterostructures with abundant catalytic active sites for enhanced methanol oxidation electrocatalysis. *J. Colloid Interface Sci.* **2023**, *630*, 570–579. [[CrossRef](#)]
54. Li, W.; Song, Z.; Deng, X.; Fu, X.-Z.; Luo, J.-L. Decoration of NiO hollow spheres composed of stacked nanosheets with CeO₂ nanoparticles: Enhancement effect of CeO₂ for electrocatalytic methanol oxidation. *Electrochim. Acta* **2020**, *337*, 135684. [[CrossRef](#)]
55. Yang, B.; Yu, Y.; Qiao, J.; Yuan, L.; Shen, X.; Hu, X. Solution plasma method for the preparation of Cu-Ni/CuO-NiO with excellent methanol electrocatalytic oxidation performance. *Appl. Surf. Sci.* **2020**, *513*, 145808. [[CrossRef](#)]

56. Luo, Q.; Peng, M.; Sun, X.; Asiri, A.M. Hierarchical nickel oxide nanosheet@nanowire arrays on nickel foam: An efficient 3D electrode for methanol electro-oxidation. *Catal. Sci. Technol.* **2015**, *6*, 1157–1161. [[CrossRef](#)]
57. Baruah, B.; Kumar, A. PEDOT: PSS/MnO₂/rGO ternary nanocomposite based anode catalyst for enhanced electrocatalytic activity of methanol oxidation for direct methanol fuel cell. *Synth. Met.* **2018**, *245*, 74–86. [[CrossRef](#)]

Disclaimer/Publisher's Note: The statements, opinions and data contained in all publications are solely those of the individual author(s) and contributor(s) and not of MDPI and/or the editor(s). MDPI and/or the editor(s) disclaim responsibility for any injury to people or property resulting from any ideas, methods, instructions or products referred to in the content.